

Contents lists available at ScienceDirect

### Computers in Biology and Medicine

journal homepage: www.elsevier.com/locate/compbiomed



## A computational pipeline towards large-scale and multiscale modeling of traumatic axonal injury

Chaokai Zhang <sup>a</sup>, Lara Bartels <sup>b</sup>, Adam Clansey <sup>c</sup>, Julian Kloiber <sup>b</sup>, Daniel Bondi <sup>c</sup>, Paul van Donkelaar <sup>d</sup>, Lyndia Wu <sup>c</sup>, Alexander Rauscher <sup>b</sup>, Songbai Ji <sup>a,e,\*</sup>

- <sup>a</sup> Department of Biomedical Engineering, Worcester Polytechnic Institute, Worcester, MA, USA
- <sup>b</sup> Department of Pediatrics, University of British Columbia, Vancouver, BC, Canada
- Department of Mechanical Engineering, University of British Columbia, Vancouver, BC, Canada
- <sup>d</sup> School of Health and Exercise Sciences, University of British Columbia, Kelowna, BC, Canada
- e Department of Mechanical Engineering, Worcester Polytechnic Institute, Worcester, MA, USA

#### ARTICLE INFO

# Keywords: Concussion Deep learning Fiber strain Displacement voxelization Multimodal analysis Multiscale modeling Traumatic axonal injury Traumatic brain injury

#### ABSTRACT

Contemporary biomechanical modeling of traumatic brain injury (TBI) focuses on either the global brain as an organ or a representative tiny section of a single axon. In addition, while it is common for a global brain model to employ real-world impacts as input, axonal injury models have largely been limited to inputs of either tension or compression with assumed peak strain and strain rate. These major gaps between global and microscale modeling preclude a systematic and mechanistic investigation of how tissue strain from impact leads to downstream axonal damage throughout the white matter. In this study, a unique subject-specific multimodality dataset from a male ice-hockey player sustaining a diagnosed concussion is used to establish an efficient and scalable computational pipeline. It is then employed to derive voxelized brain deformation, maximum principal strains and white matter fiber strains, and finally, to produce diverse fiber strain profiles of various shapes in temporal history necessary for the development and application of a deep learning axonal injury model in the future. The pipeline employs a structured, voxelized representation of brain deformation with adjustable spatial resolution independent of model mesh resolution. The method can be easily extended to other head impacts or individuals. The framework established in this work is critical for enabling large-scale (i.e., across the entire white matter region, head impacts, and individuals) and multiscale (i.e., from organ to cell length scales) modeling for the investigation of traumatic axonal injury (TAI) triggering mechanisms. Ultimately, these efforts could enhance the assessment of concussion risks and design of protective headgear. Therefore, this work contributes to improved strategies for concussion detection, mitigation, and prevention.

#### 1. Introduction

Sixty-nine million people worldwide suffer traumatic brain injury (TBI) each year [1], with ~75% of them [2], and 224 per 100 k person-years [3], sustaining a mild TBI (mTBI) often referred to as "concussion". Concussion is particularly common in athletes playing contact sports [4,5]. Diffuse axonal injury (DAI) is one of the most prominent pathologies found in all severities of TBI, including mTBI [6]. It is characterized by neuropathologically swollen axons across the brain white matter, leading to disrupted neuronal communications [7]. While DAI has been historically used to describe more severe TBI with loss of consciousness lasting 6 h or more but without a visible mass lesion [8], it

is also considered as the key substrate of concussion [9]. Given that DAI has a predisposition for white matter tracts including the corpus callosum and gray-white matter junction, it is suggested that the term, traumatic axonal injury (TAI), may be a more accurate description, especially for milder injuries with similar radiological features [10]. In this study, "TAI" is used throughout the manuscript for consistency to indicate the investigation of microscale axonal injury, regardless of the presence or severity of clinical symptoms.

The pathological mechanism of TAI is complicated; however, a clear understanding is critical to the diagnosis and clinical management [11]. There are a number of potential biomechanical triggering mechanisms for this type of injury, including microtubule (MT) disruption leading to impedance of normal axonal transport [12,13], neurofilament (NF)

<sup>\*</sup> Corresponding author. Department of Biomedical Engineering, Worcester Polytechnic Institute, Worcester, MA, USA. *E-mail address:* sji@wpi.edu (S. Ji).

#### Nomenclature

- [DAI] Diffuse Axonal Injury: A form of brain injury where widespread lesions occur in the white matter tracts of the brain, often associated with traumatic brain injuries
- [DWI] Diffusion Weighted Imaging: A type of magnetic resonance imaging that measures the diffusion of water molecules in biological tissues, such as the brain
- 3. [FE] Finite Element: A computational modeling method used to simulate and analyze complex structures, such as the human brain, under various conditions
- 4. [iMG] Instrumented Mouthguard: Mouthguard with electronic sensors to record head impacts in sports, providing data for the analysis of traumatic brain injury
- 5. [MPS] Maximum Principal Strain: A measure to quantify the maximum extent of deformation or strain in material
- 6. [MT] Microtubule: A microscopic tubular structure present in axons, involved in maintaining cell structure and transport within nerve cells
- 7. [mTBI] Mild Traumatic Brain Injury: A mild form TBI, often referred to as a concussion, representing less severe brain injuries that still may have significant neurological consequences
- 8. [NF] Neurofilament: A type of intermediate filament in neurons, providing structural support and playing a role in cell signaling
- 9. [TAI] Traumatic Axonal Injury: Injury to the brain white matter axons defined as multiple, scattered, small hemorrhagic or non-hemorrhagic lesions, together with impaired axoplasmic transport, axonal swelling, and disconnection
- 10. [TBI] Traumatic Brain Injury: A type of brain injury that occurs due to external impact, often leading to a range of physical and neurological symptoms
- 11. [WHIM] Worcester Head Injury Model: A finite element model of the human brain developed at the Worcester Polytechnic Institute. It is a subject-specific brain model that can be also warped to create subject-specific brain injury models of other individuals

compaction [14,15], axonal alteration and tau protein failure [14,16], and axolemma mechanoporation [17]. Regardless, it is generally believed that tissue-level brain deformation, when large or rapid enough, initiates the cascade of events leading to TAI [10]. It is infeasible to directly measure brain tissue or axonal deformation in vivo, especially for an injury-level insult. As a result, physics-based models of the brain have been developed across different length scales. At the global, organ level, earlier analytical models have evolved into two- and then three-dimensional finite element (FE) brain models with more complete anatomical features and refined mesh [18–20]. These models synthesize tissue structures and material properties and apply loading and boundary conditions to simulate impact, from which to derive mechanical responses such as strain, strain rate, stress, and pressure [20]. Some recent model advancements include the incorporation of brain material property anisotropy [21-23] and heterogeneity [24,25], whole-brain tractography [26-28], cerebral vasculatures [29,30], explicit gray-white matter interface [31,32] and other anatomical regions [33,34], and with improved subject-specificity [35–37] to achieve mesh convergence [38].

A primary use of these global brain models is to correlate brain responses with the occurrence of real-world brain injury, from which to establish injury risk functions or tissue injury thresholds through regression models [20,39]. However, these statistical correlations do not

infer the cause of injury. They are not sufficient to study the TAI injury mechanisms, in part, because their millimeter spatial resolution [19,20] is unable to infer how axonal structures are damaged at the microscale [7]

Mechanisms of microscale axonal damage can be investigated using axonal injury models. Earlier mathematical models consist of a bundle of MTs cross-linked by short side-arm tau proteins, e.g., with two MTs in a unit cell model [40,41] or more complete MTs arranged in a hexagonal cross-sectional pattern [42–44]. They are used to study MT bundle behaviors in steady state, quasistatic, and at higher strain/strain rate magnitudes that have the potential for MT breakage or cross-link failure in dynamic stretch loading. More sophisticated axonal FE models have also been developed to include other important cytoskeletal structures such as tau proteins, neurofilament (NF), axolemma, and myelin sheath [45–47]. These models enable the investigation of additional TAI triggering mechanisms beyond MT breakage, such as axolemma mechanoporation and failure of tau and NF.

There are at least two outstanding gaps between global and microscale model-based injury studies. First, while a global model simulation provides spatially detailed tissue responses of the entire brain, a microscale model only investigates a tiny section of a single axon through a unit cell model. Although region-specific axonal models in the corpus callosum [48] and sex-specific models [47] are also available, they remain limited to studying a tiny section of a single axon. Given that axonal stretch temporal history profiles serving as model input are expected to differ across the brain, responses from a rather small section of a single axon cannot be extended to other brain regions without fresh simulations. However, this is infeasible because of the rather high computational cost even for a single model simulation (many hours).

Second, while it is common to use real-world impact kinematics as input to a global brain model for injury analysis [20,49], microscale axonal injury models have largely been limited to using inputs with assumed peak strain and strain rate magnitudes but without an unloading or recovery phase for the axon to return to a globally undeformed, initial state [40,42,44–46,50]. Without such an unloading/recovery phase, the axonal responses may not be realistic [47] because that would prevent the reproduction of MT undulation as observed in experiment [12,13]. It is critical to apply a realistic input for axonal injury model simulations to ensure relevance to real-world injury. The lack of a systematic investigation of the biomechanical basis of concussion across the organ-to-cell length scales is, in part, because of limited multimodal data available from the same individuals in terms of impact biomechanics, neuroimaging, and clinical diagnosis of concussion.

In this study, a unique subject-specific multimodality dataset is utilized to develop an efficient and scalable computational pipeline to allow large-scale microscale injury model simulations throughout the entire white matter. The multimodality dataset contains the injurycausing impact kinematics recording as well as high-resolution neuroimaging that enables detailed white matter tractography. This largescale (i.e., throughout the entire white matter, and to be extended to various head impacts from arbitrary individuals in the future) and multiscale (i.e., from organ to cell length scales) modeling framework is necessary to enable a mechanistic investigation of TAI triggering mechanisms for real-world head impacts. Large-scale global model simulations are now possible with deep learning to dramatically improve efficiency while retaining high accuracy (e.g., from typically hours of simulation for one head impact on a high-performance computer to less than a second on a laptop [36,51-55]). This deep learning technique has been successfully applied in diverse problems such as computational biomechanics [56], diagnosis of Alzheimer's disease [57], and prediction of TBI outcomes [58], genomic data [59], and oral mucositis [60]. It is anticipated that a deep learning model will be similarly effective for a microscale injury model as well because both models use time series data as input [61]. Nevertheless, a streamlined computational pipeline is necessary to efficiently and accurately

generate inputs required for the microscale axonal injury model before developing and applying such a deep learning surrogate.

The computational pipeline employs a displacement voxelization scheme that essentially resamples the displacement field using a 3D image volume [62]. The resampling spatial resolution can be adjusted to balance accuracy and efficiency. This technique is effective at resolving the classical mesh-image mismatch problem and avoids the conventional strain tensor projection that could compromise accuracy and efficiency [27,37,63–65]. Based on the neuroimages and white matter tractography from the dataset, fiber strain profiles either in targeted regions or sampled from the entire white matter are also produced that could serve as input for downstream axonal injury models. This is important to facilitate future development of a deep learning axonal injury model to allow for large-scale and multiscale biomechanical modeling of TAI to uncover the mechanism of axonal damage at the

microscale. Ultimately, these efforts could contribute to improved safety protocols and protective equipment to better protect the brain.

#### 2. Methods

A multimodality dataset from a varsity male ice-hockey player (21 years) who sustained a diagnosed concussion at the University of British Columbia (UBC) was used for this study. Subject recruitment and data collection (approved by Research Ethics Board at UBC ID #: H21-00400) are part of a larger study to investigate prospectively and longitudinally the concussive and subconcussive mechanisms of mild traumatic brain injury. Fig. 1 shows the overall procedure of the computational pipeline. The modeling framework takes head impact kinematics as input to generate detailed strain throughout the brain for the global, organ model. The deformation field is resampled into a structured, voxelized

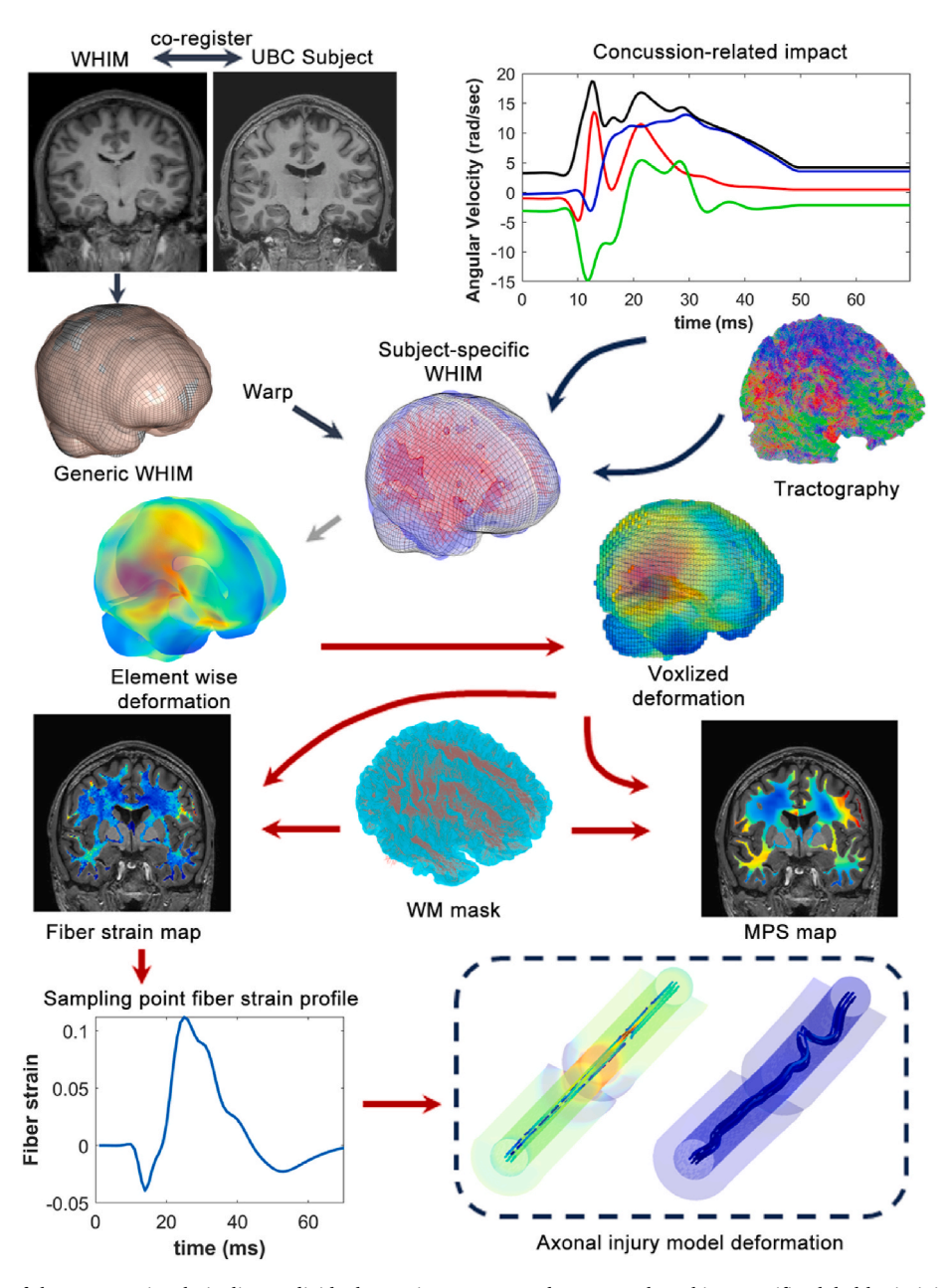


Fig. 1. Overall procedure of the computational pipeline. Individual neuroimages are used to create the subject-specific global brain injury model. It takes impact kinematics of the same concussed individual for impact simulation. The resulting voxelized deformation is combined with information from neuroimaging to generate detailed strain maps as well as temporal history of white matter fiber strain profiles in specific regions. They will next be used as input to an axonal injury model to produce a training dataset necessary to develop a deep learning surrogate in the future (hence, dashed box).

data format to greatly facilitate multimodal strain analysis. The strain profiles along white matter fiber directions will be further used as input to a cellular axonal injury model to estimate cytoskeletal damage in the future.

#### 2.1. Biomechanical data

Head impacts were recorded using a custom-fitted instrumented mouthguard (iMG; Prevent Biometrics, Minneapolis, USA) throughout the ice hockey play season. The rigid coupling between mouthguard and the upper dentition helps improve the accuracy of recorded skull impact kinematics. As a result, it is used in various contact sports, including American football [66], Rugby [67,68], and boxing [69]. Previous validation studies on the iMG showed concordance correlation coefficients of 0.97 [70] and 0.98 [71] for the accuracy of kinematics with crash test dummy headform, with positive prediction values of 96% [70] and 94% [71] based on on-field video verification. The iMG recorded impact kinematic profiles during play when any axis on the accelerometer exceeded a 5 g trigger threshold, capturing 10 ms of pre- and 40 ms post-trigger data at a sampling rate of 3.2 kHz.

Prior to season start, the subject already had 5 previously diagnosed sports related concussions. During play, the subject was diagnosed with another concussion, experiencing typical post-concussion symptoms including headache, anxiety, and difficulty in concentration but no loss of consciousness. Retrospectively, the head impact of the largest peak rotational velocity magnitude on the day of diagnosis was identified. The concussive impact was further verified by time-synchronized multiangle video recordings. Fig. 2 shows the impact kinematic profile prescribed at the head center of gravity over a duration of 50 ms. An additional 20 ms of zero acceleration (constant velocity) was appended at the end to ensure peak strains were reached in the simulation [72].

# 2.2. Neuroimage acquisition, preprocessing, and tractography reconstruction

Pre-season neuroimaging was acquired on a 3T MRI scanner (Philips Elition) equipped with a 32 channel SENSE head coil. MRI data acquired included a 3D T1 weighted scan (echo time = 4.33 ms, repetition time = 9.3 ms, isotropic voxel size of 0.8 mm) and diffusion weighted imaging (DWI; 128 diffusion directions, b = 0, 500, 1000, 2000; echo time = 95 ms, repetition time = 4250 ms, isotropic voxel size of 2 mm, 75 slices, and multi-band factor = 3). QSIPrep 0.16.1 [73] was used for neuroimage preprocessing of the T1 weighted and diffusion data as well as for tractography reconstruction. The main procedures are briefly described

below and detailed in Appendix A.

The T1-weighted image was corrected for intensity non-uniformity [74] (ANTs 2.4.0) and was used as a reference throughout the workflow. The reference was skull-stripped and spatially normalized to a template [75,76]. Cortical surfaces were reconstructed using Free-Surfer's recon-all (FreeSurfer 7.3.2 [77]) within the FMRIPrep framework [78]. DWI was denoised [79] and corrected for B1 field inhomogeneity [74]. FSL's eddy was used for head motion correction and Eddy current correction [80]. The susceptibility-induced off-resonance field was estimated using a method similar to that described in Refs. [80,81]. The DWI time-series were resampled at 2 mm isotropic spatial resolution.

For tractography, fiber orientation distributions (FODs) were estimated via constrained spherical deconvolution [82,83] using an unsupervised multi-tissue method [84,85]. FODs were intensity-normalized using mtnormalize [86]. Anatomically constrained probabilistic tractography was then performed in MRtrix3 [87,88] based on the tissue segmentations generated by Freesurfer. The resulting  $\sim\!\!10$  million streamlines were downsampled to 50 k for subsequent brain strain analysis. Finally, the T1-weighted anatomical image volume was resampled at an isotropic resolution of 1 mm for convenience in subsequent strain analyses.

#### 2.3. Subject-specific brain model

A previously developed mesh warping method [63] was used to create a subject-specific brain model based on a series of image registrations (as illustrated in Fig. 1). The subject's segmented brain was co-registered (rigid, affine, and then non-rigid) with that of the subject used to develop the anisotropic Worcester Head Injury Model (WHIM) Version 1.0 [21]. The model assumes the white matter as an anisotropic material based on tractography information from neuroimaging and an isotropic material for the gray matter. The deformation field was used to warp the WHIM mesh nodes without altering the nodal connectivity or mesh topology. The brain was 24.3% larger than the generic WHIM in volume, with scaling factors along the x, y, and z directions (posterior-to-anterior, right-to-left, and inferior-to-superior, respectively) of 1.08, 1.06, and 1.09, respectively, as determined from the affine registration. However, the subject-specific brain model has the same numbers of nodes and elements relative to the generic WHIM (56.6 k nodes and 55.1 k hexahedral elements for the brain, respectively; Fig. 3).

The generic WHIM has been extensively validated across a wide range of blunt conditions, including relative brain-skull displacement and sparse marker-based strain in high and mid-rate cadaveric impacts,

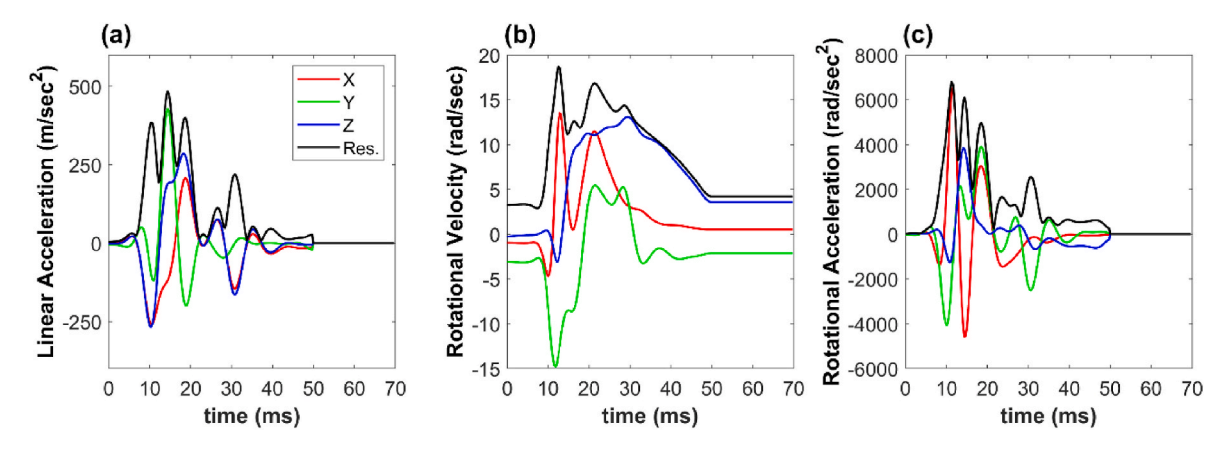


**Fig. 2.** Linear acceleration (a), rotational velocity (b), and rotational acceleration (c) profiles believed to be related to the diagnosed concussion for the subject (largest peak rotational velocity magnitude among recorded impacts on the day of concussion). An additional 20 ms of zero acceleration is appended at the end of impact to ensure peak strains are reached in simulation. Discontinuity in acceleration is automatically smoothed in simulation to avoid any numerical artefact. The resultant linear acceleration, rotational velocity, and rotational acceleration of the impact are 14.7 m/s², 18.7 rad/s, and 6670.2 rad/s², respectively. The varying magnitudes of kinematics across the three axes over time suggest complex head motion during impact.

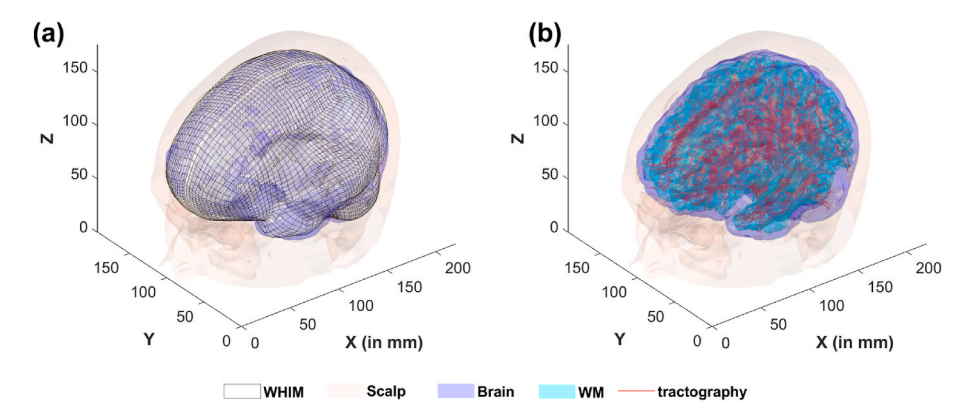


Fig. 3. (a) The subject-specific global brain model, with the brain outer surface mesh overlaid against the brain and scalp surfaces segmented from the individual's T1-weighted neuroimages. (b) Randomly selected tractography streamlines (5% of the total of 50 k) overlaid against surface renderings of the white matter, brain parenchyma and scalp based on neuroimage segmentation in the brain model space.

as well as full-field strains from *in vivo* head rotations [89]. For marker-based strain validation against mid-rate impacts simulating those in contact sports, the model achieved a peak strain ratio of  $0.94 \pm 0.30$  relative to those in 12 experiments (a ratio of  $1.0 \pm 0.0$  would be "perfect", albeit experimental errors, themselves, should not be ignored [90]). These validations are important to ensure sufficient confidence in downstream axonal injury model simulations because fiber strain profiles are directly used as input [47,48].

#### 2.4. Voxelwise strains via displacement field voxelization

Both subject-specific neuroimages and FE mesh discretize the brain. However, their mismatch could pose some challenges in effective multimodal injury analysis. Here, a displacement voxelization scheme was adopted to resolve the issue [62]. First, voxel corner nodes of the subject's T1-w images in the model space were used to interpolate (via "scatteredInterpolant.m" in Matlab) relative brain-skull displacement from the FE model simulation at every time frame for output (temporal resolution of 1 ms). This led to a high-dimensional structured image representation of the simulated spatiotemporal deformation (with a dimension of  $194 \times 230 \times 194$ ). Voxelwise strain tensors can then be determined via standard shape functions with high efficiency, as the Jacobian matrix involved is degenerated into an identity matrix for isotropic voxels [62]. Voxelwise maximum principal strain (MPS) was then determined as the maximum eigenvalue of the strain tensor for each voxel at the centroid (with a dimension of  $193 \times 229 \times 193$ ).

To determine fiber strain, displacement at every white matter fiber sampling point ( $\sim$ 4.47 million points from 50 k streamlines) was first calculated from the voxelized displacement field through standard hexahedral element shape functions [62]. The displacement difference between two adjacent fiber sampling points readily determined the

stretch at their mid-point, which was defined as the fiber strain sampling point. This process was repeated at every time point, from which peak fiber strain was calculated. Next, embedding voxels for all fiber strain sampling points were identified to compute voxelwise weighted averages of peak fiber strains [26], including those from "major" or crossing fibers (illustrated in Fig. 4). The white matter mask was finally applied to remove artefacts due to spurious tractography.

#### 2.5. Scalability of the computational pipeline

To demonstrate the scalability of the computational pipeline to balance accuracy and efficiency, the T1-weighted neuroimages (of 1 mm isotropic resolution) were systematically downsampled to an isotropic resolution of 2 mm and 4 mm. This was achieved by conveniently skipping 1 or 3 consecutive indices along each direction of the three-dimensional matrix data, respectively. The same process was repeated to determine voxelwise MPS and fiber strain at the corresponding spatial resolutions. Given that the same tractography was used for fiber strain  $(\varepsilon_n)$ , its accuracy was quantitatively compared against the baseline obtained from the 1 mm resolution  $(\varepsilon_{n\_baseline})$  in terms of relative percentage differences (Eqns. (1) and (2)):

$$\varepsilon_{n,error}^{i} = \left| \varepsilon_{n\_basline}^{i} - \varepsilon_{n}^{i} \right| \tag{1}$$

relative percentage difference = mean 
$$\left(\sum_{i=1}^{n} \frac{\varepsilon_{n,error}^{i}}{\varepsilon_{n,basline}^{i}}\right) \times 100\%$$
 (2)

where i represents the sampling point number and n is the total number. In addition, the computational efficiency for each step involved was also compared. Comparing the accuracy of voxelwise MPS was not feasible, as voxel centroids did not align among the spatial resolutions

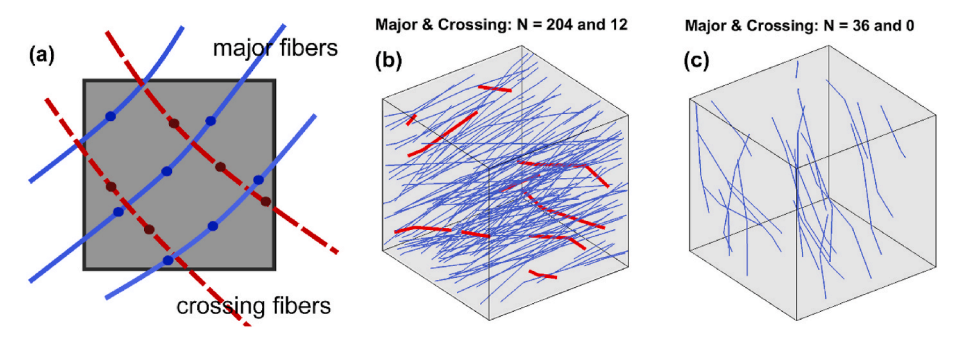


**Fig. 4.** (a) Illustration of the "major fibers" within the voxel with the largest number of streamlines enclosed and crossing fibers of less streamlines (if present). Voxelwise fiber strain is determined through a weighted averaging process based on the number of fiber strain sampling points (dots). A 3D resampling voxel with (b) the most major fibers or (c) no crossing fibers are reported for the subject (the numbers of major and crossing fibers are shown in figure).

considered.

#### 2.6. Representative white matter fiber strain profiles

The computational pipeline produced dense fiber strain profiles throughout the white matter. Typical locations of TAI include graywhite matter interface (especially in the frontotemporal regions) and corpus callosum [6,91]. To demonstrate the convenience of conducting a multimodal injury analysis using voxelized deformation and information from neuroimaging, representative fiber strain profiles in these areas were also reported for illustration. The corpus callosum region has been defined in the WHIM space, but the white matter mask was given by the individual's neuroimages (isotropic resolution of 1 mm). Voxels near the gray-white matter interface were identified by subtracting the binary mask by a slightly eroded image volume (with an empirical structural element size of 4). These regions were used to constrain the identification of fiber strain sampling points.

#### 2.7. Diverse fiber strain profiles

Neighboring fiber strains within the same tract are expected to be similar because of the continuous displacement field and similar streamline orientations in the neighborhood (Fig. 3; unless a sharp turn occurs). Intuitively, however, *diverse* rather than similar training samples are favored when developing a deep learning axonal injury model to maximize generalizability. Diverse fiber strain inputs would also provide the most comprehensive sampling to facilitate neural network training, which would lead to fewer training samples necessary to reduce the computational cost for their generation [61].

To identify diverse fiber strain profiles throughout the white matter, impact-induced relative brain-skull displacement from simulation was resampled at an empirical isotropic resolution of 6 mm. This led to N = 5698 voxels for the brain, from which N = 2432 contained white matter. The latter was consistent with the typical number of training samples for a deep learning global brain model [61]; hence, the chosen resampling resolution. For each voxel containing white matter, the fiber strain sampling point of the largest peak fiber strain magnitude was identified. The coarse resampling resolution helped maintain (albeit not necessarily  $\it ensure$ ) distinct spatial locations among the identified fiber strain sampling points. However, it did not influence the "accuracy" of fiber strains as they were determined with a resampling resolution of 1 mm.

Next, pairwise cross-correlation coefficients between the identified fiber strain profiles were calculated. The coefficients had a range from -1 (most diverse) to 1 (most similar). The pair with the lowest correlation coefficient were determined and removed from subsequent

consideration. This process was repeated until all pairs were scrutinized. The resulting sequence effectively established a descending order of diverse pairwise fiber strain profiles. Fig. 5 illustrates the adjacency matrix with cross-correlation coefficients for 50 randomly selected fiber strain profiles (vs. N=2938 to improve visualization).

#### 3. Data analysis

The computational framework allows processing simulated biomechanical data (displacement and strain) using a neuroimaging data structure at an arbitrary sampling resolution. In this study, we compared the computational efficiency and accuracy of dense white matter fiber strains across different spatial sampling resolutions based on the same tractography. Next, representative fiber strain profiles were reported at the gray-white matter interface and in the corpus callosum, regions known to be particularly vulnerable to TAI. Finally, the diverse fiber strain profiles were also analyzed using the distribution of pairwise cross-correlation coefficients across the entire white matter. This was important to identify training samples necessary to develop a deep learning axonal injury model in the future.

The impact was simulated using the anisotropic WHIM V1.0 in SIMULIA Abaqus/Explicit (version 2022; double precision) on multicore Windows Terminal Servers using 20 cores (Intel Xeon Gold 6348, 2.4 GHz, 128 GB memory). All data analyses were conducted in MATLAB (R2020a; Mathworks, Natick, MA) on a desktop computer (AMD 3950  $\times$  16 cores, 64 GB RAM). To create the subject-specific brain models, the most time-consuming step was brain extraction ( $\sim$ 5.6 h; "recon-all" in FreeSurfer [77]). The remaining registrations and mesh warping took 3.5 min in total.

#### 4. Results

#### 4.1. Voxelwise strains

Fig. 6 shows voxelized relative brain-skull displacement magnitudes (when the corpus callosum fiber strain reached its first major peak; Fig. 8) on three neuroimaging planes and the corresponding voxelwise peak MPS and peak fiber strains. The three displacement components are reported in **Appendix B** (Figure A1), where positive and negative displacements are both present on the same imaging planes, demonstrating a "sloshing" motion. The planes for displacement and strains differed by half a voxel spacing as the former were given on voxel corner nodes while strains were on voxel centroids. The subject-specific neuroimage was slightly misaligned; hence, some left-right *asymmetry* observable on the axial image plane. The displacement magnitude, MPS,

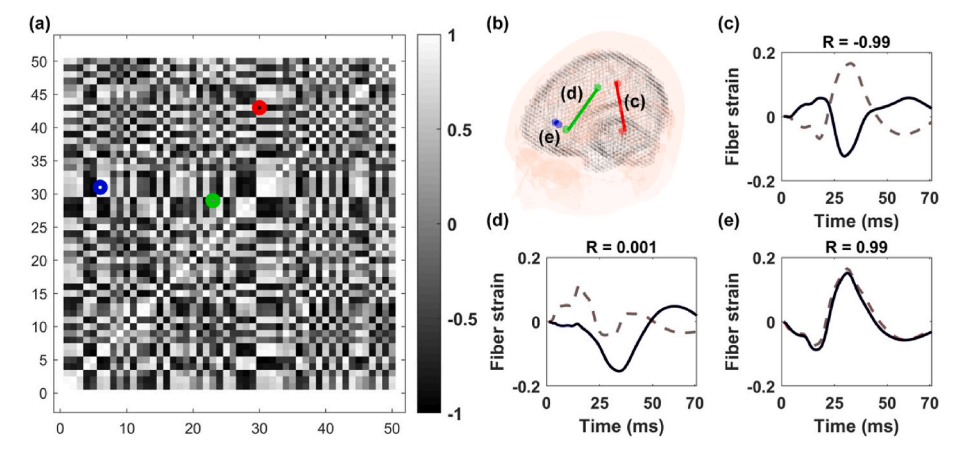


**Fig. 5.** Illustration of diverse fiber strain profiles based on pairwise cross-correlation coefficient shown as an adjacency matrix. The scores have a range from -1 (most diverse) to 1 (most similar), which are used to identify distinct fiber strain pairs. Three pairs are illustrated, with their spatial locations within the voxelized brain surface shown (at an isotropic voxel resolution of 6 mm). Not surprisingly, the two spatially close sampling points have rather similar fiber strain profiles (*R* of 0.99).

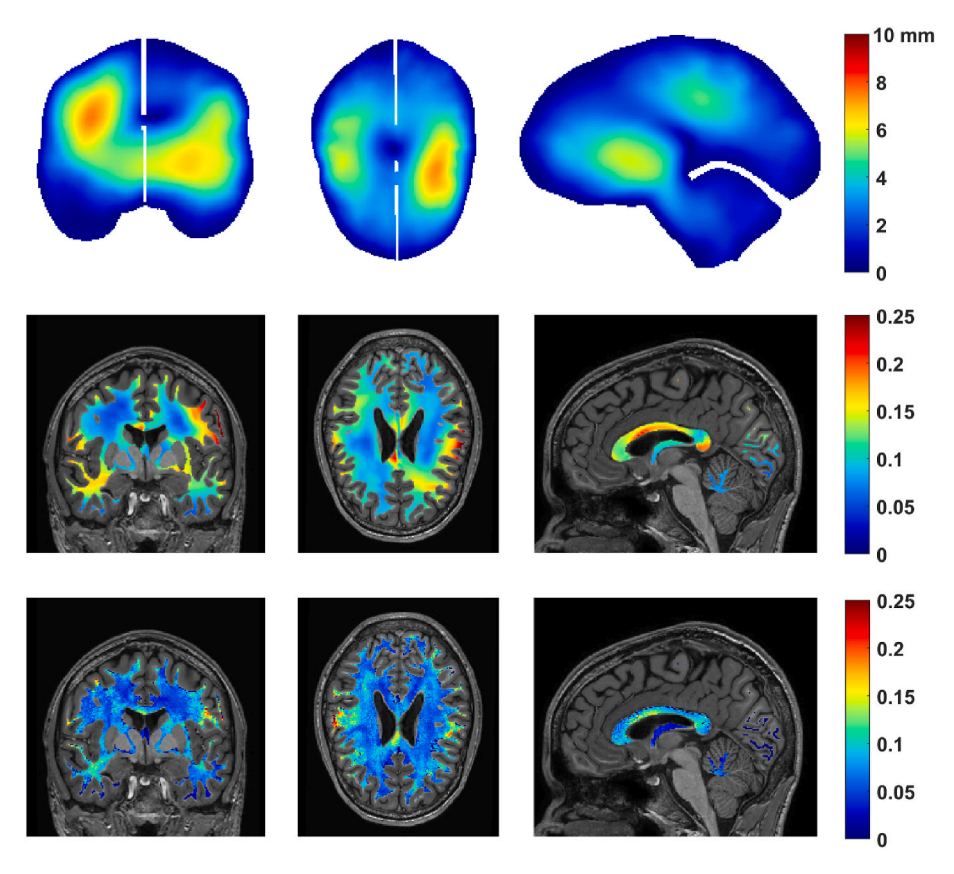


Fig. 6. Voxelized magnitude of relative brain-skull displacement from impact simulation (top row) at the time when corpus callosum fiber strain reached its first major peak (~31 ms; see Fig. 8) in coronal (left), axial (middle column) and para-sagittal (right) planes, along with the corresponding voxelwise peak MPS (second row) and averaged fiber strains (bottom row).

and fiber strains shown here are all invariant to the coordinate system used.

Fig. 7 compares voxelwise relative brain-skull displacement, peak MPS and fiber strains at three voxel resampling resolutions. Their accuracy in peak fiber strains and computational efficiency relative to the baseline are compared in Table 1. The white matter region "grew" when increasing the sampling voxel size, for example, by 16.2% and 45.7% relative the white matter volume ratio of 24.6% at the 1 mm when instead, resampled at 2 mm and 4 mm, respectively. This was because a larger voxel is considered as "white matter" even if only a partial volume (from the smaller voxels) was designated as white matter.

#### 4.2. MPS of the whole brain and corpus callosum fiber strain

Fig. 8 shows the temporal profiles of MPS of the whole brain and corpus callosum fiber strain overlaid on those of the normalized resultant rotational velocity and acceleration profiles. It can be observed that the former largely followed the shape of the resultant rotational velocity but not the latter, as indicated by their corresponding cross-correlation coefficient of 0.83 and -0.52, respectively (p<0.01 for both). Their cross-correlation coefficients relative to the resultant rotational acceleration profile were 0.44 (p<0.01) and -0.20 (p=0.089), respectively. The first major peak of MPS of the whole brain virtually coincided with the peak of the resultant rotational velocity/acceleration profiles, but there was a 18.5 ms delay for the first major peak of corpus callosum fiber strain.

#### 4.3. Representative fiber strain profiles

As an illustration, representative fiber strain profiles are shown near the gray-white matter interface in two contralateral regions and in the corpus callosum (Fig. 9). They were identified based on segmentation of individual neuroimages, and the region defined by the WHIM model, respectively. It was also observed that the left and right hemispherical regions experienced tension and compression in opposite phases. This was expected given the nearly incompressible brain, that tissue in different regions will experience tension and compression at the same time to maintain a nearly constant volume.

#### 4.4. Diverse fiber strain profiles

Finally, the distribution of pairwise cross-correlation coefficients is shown (Fig. 10). Because the fiber strain profile selection strategy favored the identification of more diverse profiles from the  $2432 \times 2432$  adjacency matrix (Fig. 4), most of the identified pairs from the  $2432 \times 2432$  samples or 1216 pairs had a cross-correlation coefficient below zero (i. e., 840 out of the 1216 pairs, or 69%). From these, 96% of them clustered below -0.8 (e.g., 804 pairs out of the 840 pairs). For each histogram bin, a representative pair is shown.

#### 5. Discussion

A multiscale modeling framework unifying a global and a microscale injury model is critical for a mechanistic investigation of TAI. The framework would bridge the gaps among external head impact, tissue strain, and microscale axonal damage at the cellular level, which cannot be achieved otherwise using either model, alone. However, a large-scale simulation is necessary to estimate axonal structural damage in specific anatomical regions or the entire white matter. Injury biomechanical findings can then be assessed by structural, functional, and physiological biomarkers measured at the tissue and organ level. To further enable population-based TBI and TAI investigations such as deriving injury risk

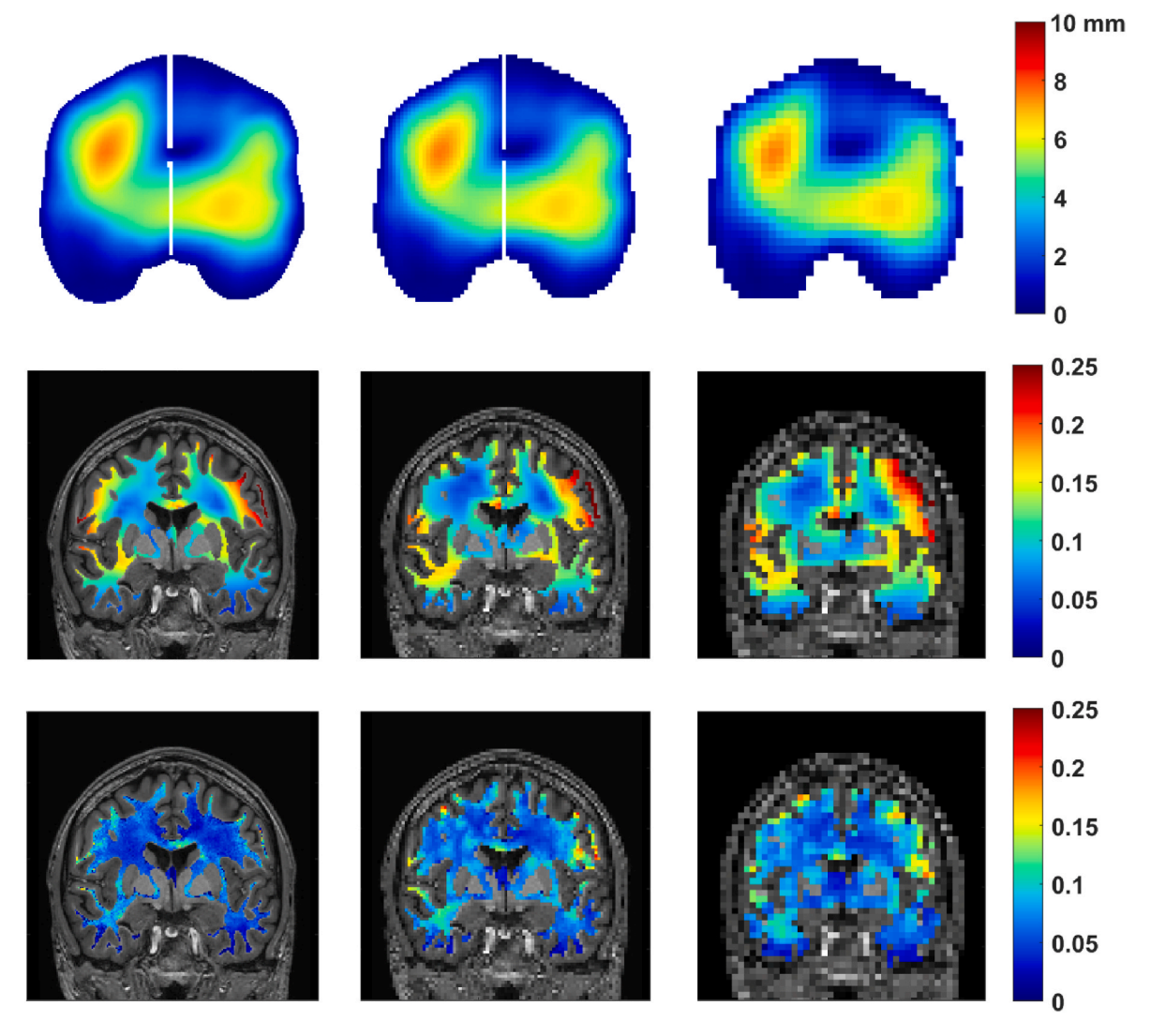


**Fig. 7.** Comparison of voxelwise displacement magnitude, peak MPS, and peak fiber strains at three sampling resolutions on a coronal plane (from left to right columns: isotropic resolution of 1 mm, 2 mm, and 4 mm, respectively). With the increase in resampling voxel size, the white matter region appears "growing", because a larger voxel is considered as "white matter" even if only a partial volume is designated as white matter.

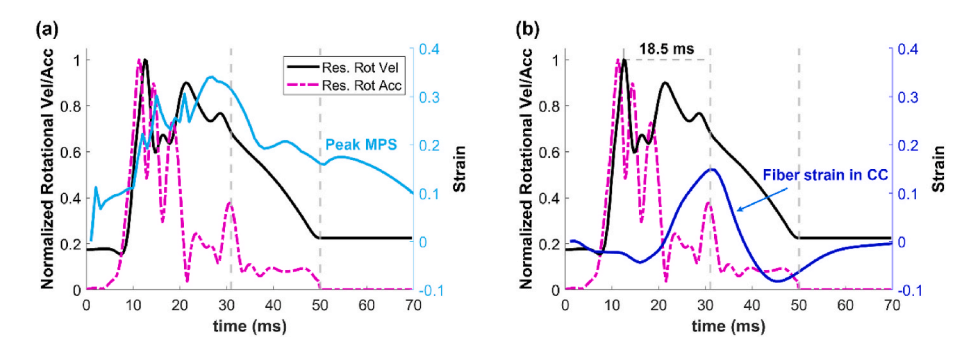


**Fig. 8.** Temporal profiles of MPS of the whole brain (a) and corpus callosum fiber strain (b) overlaid against the resultant rotational velocity and acceleration profiles (both normalized to provide shape only). The vertical dashed line at 31ms indicates the time when the corpus callosum fiber strain reached its first major peak (of tension). The one at 50 ms indicates the time window of the impact recording.

functions and thresholds, it is also important to extend the multiscale modeling framework across head impacts and across individuals as well due to the cumulative effects of subconcussive impacts on the onset of sports-related concussion. A large-scale and multiscale mechanistic modeling of TAI could significantly enhance state-of-the-art approaches to improving the detection, mitigation, and prevention of TBI in the

future. Large-scale impact modeling for the global brain is now possible through deep learning [20]; but a deep learning surrogate for an axonal injury model has yet to be developed.

The computational pipeline established in this study is necessary for the development and application of a deep learning axonal injury model. The pipeline integrates individualized neuroimages to produce

**Table 1**Comparison of fiber strain error (in percentage, %) and computational efficiency (in sec) for three displacement resampling resolutions relative to those from the resampling resolution of 1 mm.

Sampling spatial isotropic resolution	1 mm	2 mm	4 mm
Error relative to baseline	N/A	6.4%	14.2%
Voxelwise displacement (sec)	130.8	19.7	3.3
Voxelwise MPS (sec)	37.6	8.0	1.3
Voxelwise fiber strain (sec)	367.2	60.8	12.2
Total time (sec)	535.6	88.5	16.8
Time reduction relative to baseline	N/A	83.4%	96.9%

voxelwise relative brain-skull displacement and strain from a subject-specific global model. The resulting high-dimensional structured deformation field allows convenient determination of white matter fiber strains along dense tractography. The temporal fiber strain profiles would then serve as inputs to a microscale axonal injury model to estimate the extent of axonal structural damage such as MT, tau, and NF

breakage, either in specific anatomical regions such as the gray-white matter interface and corpus callosum (Fig. 9) or the entire white matter (Fig. 10). The diverse fiber strain profiles are expected to facilitate the generation of training samples through direct axonal model simulations for a deep learning surrogate. Once developed, the deep learning model could dramatically improve simulation efficiency with high accuracy, similar to the global model as both use time series data, either the impact rotational kinematics profile or axonal stretch time history, as model inputs.

#### 5.1. Computational efficiency

The computational pipeline is scalable. When subject-specific neuroimages are available, the image volume can be transformed into FE model space to resample relative brain-skull displacement at the voxel corner nodes. This strategy ensures a one-to-one direct correspondence between image voxels and voxelwise strains, which would facilitate biomechanics-neuroimaging multimodal injury analysis. When

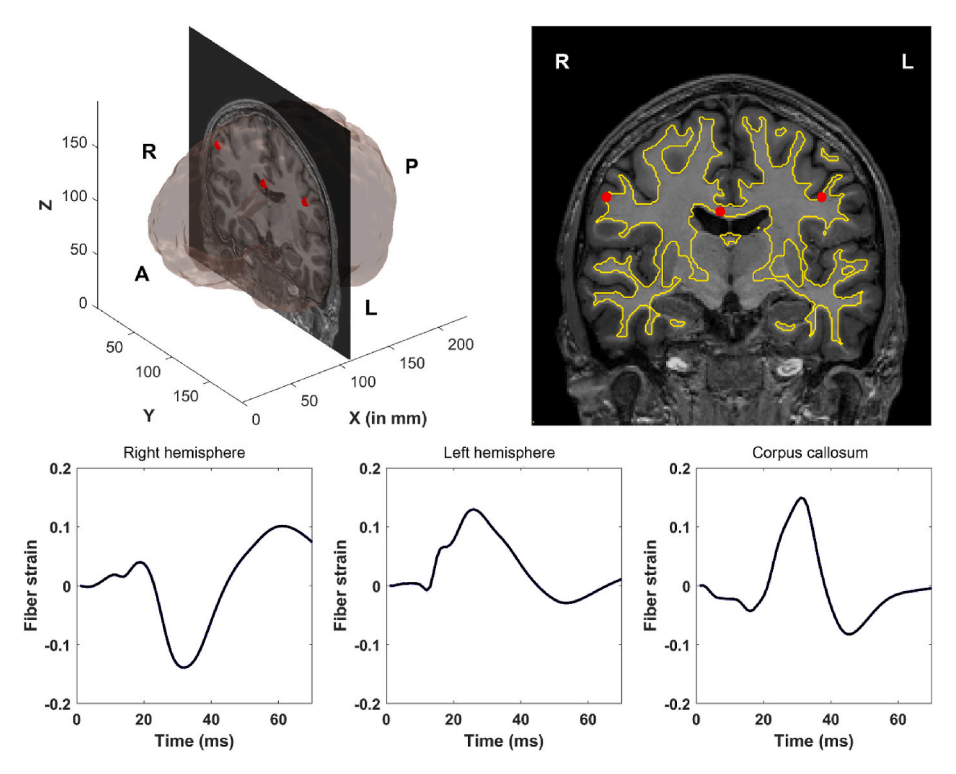


Fig. 9. Representative fiber strain profiles near the gray-white matter interface in two contralateral regions and in the corpus callosum for a concussive head impact recorded for a male ice-hockey player. All the fiber strain major peaks occur about the same time, with some delay relative to the major peak in the head rotational velocity profile shown in Fig. 8. The two fiber strain profiles in the contralateral regions are opposite in phase, showing major peaks of compression for (a) and tension for (b), respectively.

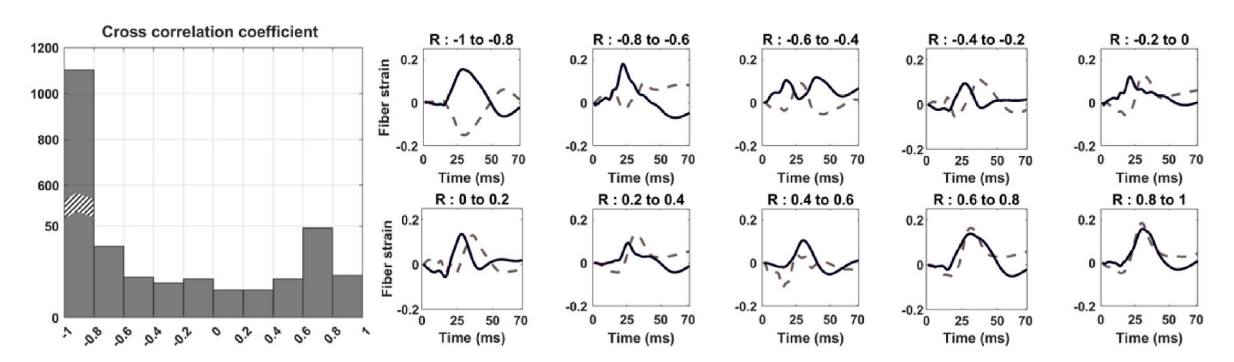


Fig. 10. Histogram distribution of the cross-correlation coefficients between pairwise fiber strain profiles and sample pairs in each bin. Most of the pairs identified have a low value of cross-correlation coefficient, suggesting the effectiveness of the identification process for diverse profiles.

individual neuroimages are not otherwise available, a generic grid can be used for response resampling [36,53]. In both cases, the voxel spatial resolution can be adjusted to balance accuracy and efficiency in response resampling (Fig. 7).

The computational efficiency dramatically improved with the increase of the deformation resampling voxel size. When the sampling voxel size increased from 1  $\text{mm}^3$  to 2  $\text{mm}^3$  (4  $\text{mm}^3$ ), a reduction of 83.4% (96.9%) in computation time was achieved, which also led to a relative error in fiber strain of 6.4% (14.2%) (Table 1). These results suggest that a sampling resolution of 2  $\text{mm}^3$  might offer an appropriate tradeoff between accuracy and efficiency.

Outside of the post-simulation processing, brain extraction was the most time-consuming operation (>5.6 h) when developing the subject-specific brain model. The FSL BET package could dramatically improve efficiency (4.6 s vs. >5.6 h). However, the presence of residual tissues such as the dura, nasal concha, and sphenoid sinus precluded proper registrations with the brain from the baseline WHIM when developing the subject-specific model. On the other hand, the recent 'fastsurfer' toolbox [92,93] may mitigate these challenges and can be applied in the future for development of subject-specific models.

#### 5.2. Fiber strain profiles

Given the near incompressibility of the brain, it is expected that some white matter fibers will experience tension while others will experience compression at a given time point (Figs. 9 and 10) so that the total brain volume remains nearly unchanged. Some compressibility is expected for the intact brain within the skull [94–96], which was enabled by using an elastic cap in the foramen magnum [63]. Mechanical responses of axons differ greatly in tension and compression [42,97]. Therefore, when developing a deep learning surrogate, it is important that the training samples include both tension- and compression-dominant profiles to maximize generalizability.

For this reason, a strategy was designed to identify a diverse range of fiber strain profiles across white matter. The coarse sampling (of 6 mm) purposefully divided the brain into relatively distinct regions to minimize the chance of selecting similar profiles between fiber strains, as only one strain profile was selected from each voxel. Peak fiber strain magnitude was used for the identification, because higher, rather than lower, fiber strain magnitudes are likely more relevant to axonal damage; thus, they were intended to contribute to the deep learning training samples. Similar fiber strain profiles could still be selected for two neighboring voxels when peak strains occurred near the voxel boundary. However, they can be detected by the pair-wise cross-correlation strategy, which favored the selection of more diverse fiber strain profiles (Fig. 5).

The strategy seemed effective, as 90% of the pairwise fiber strains had a cross-correlation coefficient between -1 and -0.8 (1103 out of 1216 pairs; Fig. 10). Nevertheless, given that only one fiber strain was selected from each voxel when identifying the diverse fiber strain profiles, crossing fibers were effectively excluded in the process (Fig. 4). However, they can be easily incorporated as necessary, e.g., if the resulting deep learning model does not sufficiently generalize. The diverse range of axonal fiber strain profiles (Fig. 10) provides rather rich characteristics of temporal shapes and magnitudes of fiber strains across the brain, both of which strongly affect axonal micromechanical behaviors. They offer much improved insight into axonal damage than peak fiber strain magnitude, alone.

In comparison, axonal injury model simulations have been largely limited to using a simplistic stretch profile as the loading condition for input to date, for example, pure tension or pure compression with a fixed strain peak magnitude or strain rate [42,97]. However, they are not realistic because they do not contain a "recovery phase" for the strain to return to an initial, undeformed state given that no residual strain is anticipated in a live human brain after mild impact. Not all fiber strain profiles illustrated in this study returned to a "zero strain state" within

the impact temporal window due to limitations with the impact kinematic data. Nonetheless, it was common that both tension and compression were present in fiber strain profiles, irrespective of the order of the two phases. This reflects a "sloshing" motion of the brain parenchyma inside the skull during impact, as expected. Regardless, the diverse fiber strain profiles may serve as a database for more realistic loading conditions when investigating axonal dynamic responses in the future, using either mathematical or computational FE models.

#### 5.3. Biomechanics of brain strain

The temporal profile of the MPS of the whole brain largely followed that of the resultant rotational velocity (cross-correlation coefficient of 0.83). However, this was not the case for the fiber strain profile in the corpus callosum (cross-correlation coefficient of -0.52; Fig. 8). Apparently, the MPS of the whole brain was much more influenced by impact kinematics than strain deep in the brain. For the impact simulation in this study using WHIM, MPS of the whole brain usually occurred near the brain surface, due to tissue tethering through the boundary condition at the brain-skull interface (sharing nodes via the cerebrospinal fluid layer [63]). Therefore, any change in head rotational velocity would be immediately translated into strains in this area. For the corpus callosum, however, it takes time for the shear wave to travel from the brain-skull surface to deep regions. The peak-to-peak time of 18.5 ms was slightly larger than that of 14 ms reported before [72], which was likely, in part, a result of the larger brain studied here.

The time-delay in corpus callosum strain relative to impact kinematics suggests that strain in deep brain regions may not reach peak during the given time window, even if the kinematic peak has been captured. For the simulated head impact, the peak kinematics occurred early in the time window. Therefore, the second peak of corpus callosum fiber strain (in compression) was captured even without the additional 20 ms duration (Fig. 8b). Nevertheless, the additional simulation time allowed the fiber strain to attempt to return to a "zero strain", which would be more realistic for subsequent axonal injury modeling [47].

#### 6. Limitations and future work

While this study is a critical step towards large-scale and multiscale brain injury modeling, additional development is necessary. In particular, a deep learning-based microscale axonal injury model is required to dramatically reduce FE model simulation runtime. The technique is effective for a global model, e.g., reducing hours of impact simulation on a high-end computing platform to under a second on a regular laptop, and with high accuracy [36,51–53]. A similar result is anticipated for the microscale axonal injury model because both models use time series data, either impact kinematic profiles or axonal stretch history [47,48], as input. Nevertheless, a large training sample is expected to train a neural network for a desired accuracy. A diverse set of fiber strain profiles would facilitate its development.

The diverse fiber strain profiles identified in this study from a single head impact simulation may still not be sufficient to represent those from diverse head impacts and individuals. To generalize the training data across impacts and subjects, the same computational pipeline can be applied to a range of global model simulations, for which a deep learning surrogate is already available to instantly generate spatiotemporal responses for a generic brain model [53], and in a convenient voxelized data structure [62].

#### 7. Conclusion

Using a unique subject-specific multimodality dataset from a male concussed ice-hockey player, this study develops an efficient and scalable computational pipeline to generate voxelized deformation field over time. The structured, voxelized data format allows accurate and efficient determination of voxelwise maximum principal strains at voxel

centroids as well as white matter fiber strains for embedded tractography. The spatial resolution of the voxelized deformation field (displacement and strain) can be adjusted, and an isotropic resolution of 2 mm was found to provide a reasonable balance between accuracy and efficiency. The voxelized deformation also facilitates seamless multimodal biomechanical analysis in key anatomical regions, such as graywhite matter interface and corpus callosum as examples in this study.

The computational pipeline is critical for producing diverse fiber strain profiles necessary for the development and application of a deep learning axonal injury model in the future. In turn, these efforts would allow large-scale (i.e., across the entire white matter region, head impacts, and individuals) and multiscale (i.e., from organ to cell length scales) modeling to investigate the mechanisms of traumatic axonal injury (TAI). By bridging gaps between global and microscale modeling of TAI, this study contributes to improved strategies for concussion detection, mitigation, and prevention.

#### CRediT authorship contribution statement

Chaokai Zhang: Conceptualization, Data curation, Formal analysis, Methodology, Software, Validation, Visualization, Writing – original draft, Writing – review & editing. Lara Bartels: Data curation, Formal analysis, Methodology, Software, Writing – review & editing. Adam Clansey: Data curation, Investigation, Resources, Writing – review & editing. Julian Kloiber: Data curation, Investigation, Resources. Daniel Bondi: Data curation, Investigation, Resources. Paul van Donkelaar: Funding acquisition, Investigation, Supervision, Writing – review & editing. Lyndia Wu: Funding acquisition, Investigation, Supervision, Writing – review & editing. Songbai Ji: Conceptualization, Data curation, Funding acquisition, Investigation, Software, Supervision, Writing – original draft, Writing – review & editing.

#### Declaration of competing interest

None Declared.

#### Acknowledgements

Funding is provided by the National Science Foundation (NSF) under Grant No. 2114697 and the Canadian Institutes of Health Research (CIHR) Project No. 436806. The funding sources have no role in study design or publication.

#### Appendix A. Supplementary data

Supplementary data to this article can be found online at https://doi.org/10.1016/j.compbiomed.2024.108109.

#### References

- [1] M.C. Dewan, A. Rattani, S. Gupta, R.E. Baticulon, Y.C. Hung, M. Punchak, A. Agrawal, A.O. Adeleye, M.G. Shrime, A.M. Rubiano, J.V. Rosenfeld, K.B. Park, Estimating the global incidence of traumatic brain injury, J. Neurosurg. 130 (2019) 1080–1097. https://doi.org/10.3171/2017.10.JNS17352.
- [2] S.R. Laker, Epidemiology of concussion and mild traumatic brain injury, PM&R. 3 (2011) S354–S358, https://doi.org/10.1016/j.pmrj.2011.07.017.
- [3] R. Nguyen, K.M. Fiest, J. McChesney, C.S. Kwon, N. Jette, A.D. Frolkis, C. Atta, S. Mah, H. Dhaliwal, A. Reid, T. Pringsheim, J. Dykeman, C. Gallagher, The international incidence of traumatic brain injury: a systematic review and meta-analysis, Can. J. Neurol. Sci. 43 (2016) 774–785, https://doi.org/10.1017/CJN.2016.290.
- [4] T.P. Dompier, Z.Y. Kerr, S.W. Marshall, B. Hainline, E.M. Snook, R. Hayden, J. E. Simon, Incidence of concussion during practice and games in youth, high school, and collegiate American football players, JAMA Pediatr. 169 (2015) 659–665, https://doi.org/10.1001/jamapediatrics.2015.0210.
- [5] R. Graham, F.P. Rivara, M.A. Ford, C.M. Spicer, R. Graham, Sports-Related Concussions in Youth, 2014, https://doi.org/10.1001/jama.2013.282985.

- [6] V.E. Johnson, W. Stewart, D.H.D.H. Smith, Axonal pathology in traumatic brain injury, Exp. Neurol. 246 (2013) 35–43, https://doi.org/10.1016/j. expneurol.2012.01.013.
- [7] J.M. Meythaler, J.D. Peduzzi, E. Eleftheriou, T.A. Novack, Current concepts: diffuse axonal injury-associated traumatic brain injury, Arch. Phys. Med. Rehabil. 82 (2001) 1461–1471, https://doi.org/10.1053/apmr.2001.25137.
- [8] T. Gennarelli, Mechanisms of brain injury, J. Emerg. Med. 11 (Suppl 1) (1993) 5–11.
- [9] D.H. Smith, W. Stewart, 'Concussion' is not a true diagnosis, Nat. Rev. Neurol. 16 (2020) 457–458, https://doi.org/10.1038/S41582-020-0382-Y.
- [10] G.F. Bruggeman, I.K. Haitsma, C.M.F. Dirven, V. Volovici, Traumatic axonal injury (TAI): definitions, pathophysiology and imaging—a narrative review, Acta Neurochir. 163 (2021) 31, https://doi.org/10.1007/S00701-020-04594-1.
- [11] J. Ma, K. Zhang, Z. Wang, G. Chen, Progress of research on diffuse axonal injury after traumatic brain injury, Neural Plast. (2016), https://doi.org/10.1155/2016/ 0746313
- [12] M.D. Tang-Schomer, V.E. Johnson, P.W. Baas, W. Stewart, D.H. Smith, Partial interruption of axonal transport due to microtubule breakage accounts for the formation of periodic varicosities after traumatic axonal injury, Exp. Neurol. 233 (2012) 364–372, https://doi.org/10.1016/j.expneurol.2011.10.030.
- [13] M. Tang-Schomer, A. Patel, P. Baas, D. Smith, Mechanical breaking of microtubules in axons during dynamic stretch injury underlies delayed elasticity, microtubule disassembly, and axon degeneration, Faseb. J. 24 (2010) 1401–1410.
- [14] D.G. Siedler, M.I. Chuah, M.T.K. Kirkcaldie, J.C. Vickers, A.E. King, Diffuse axonal injury in brain trauma: insights from alterations in neurofilaments, Front. Cell. Neurosci. 8 (2014) 1–10, https://doi.org/10.3389/fncel.2014.00429.
- [15] C.R. Marmarou, S.A. Walker, C.L. Davis, J.T. Povlishock, Axonal neurofilament compaction and impaired axonal, J. Neurotrauma 22 (2005) 1066–1080.
- [16] A. Katsumoto, H. Takeuchi, F. Tanaka, Tau pathology in chronic traumatic encephalopathy and Alzheimer's disease: similarities and differences, Front. Neurol. 10 (2019), https://doi.org/10.3389/FNEUR.2019.00980/FULL.
- [17] D. Kilinc, G. Gallo, K.A. Barbee, Mechanically-induced membrane poration causes axonal beading and localized cytoskeletal damage, Exp. Neurol. 212 (2008) 422–430, https://doi.org/10.1016/j.expneurol.2008.04.025.
- [18] K.H. Yang, J. Hu, N.A. White, A.I. King, C.C. Chou, P. Prasad, Development of numerical models for injury biomechanics research: a review of 50 years of publications in the Stapp Car Crash Conference, Stapp Car Crash J 50 (2006) 429–490, https://doi.org/10.4271/2006-22-0017.
- [19] A. Madhukar, M. Ostoja-Starzewski, Finite element methods in human head impact simulations: a review, Ann. Biomed. Eng. 47 (2019) 1832–1854, https://doi.org/ 10.1007/s10439-019-02205-4.
- [20] S. Ji, M. Ghajari, H. Mao, H. Kraft, Reuben, M. Hajiaghamemar, M.B. Panzer, R. Willinger, M.D. Gilchrist, S. Kleiven, J.D. Stitzel, Use of brain biomechanical models for monitoring impact exposure in contact sports, Ann. Biomed. Eng. 50 (2022) 1389–1408, https://doi.org/10.1007/s10439-022-02999-w.
- [21] W. Zhao, S. Ji, White matter anisotropy for impact simulation and response sampling in traumatic brain injury, J. Neurotrauma 36 (2019) 250–263, https://doi.org/10.1089/neu.2018.5634.
- [22] D. Sahoo, C. Deck, R. Willinger, Development and validation of an advanced anisotropic visco-hyperelastic human brain FE model, J. Mech. Behav. Biomed. Mater. 33 (2014) 24–42, https://doi.org/10.1016/j.jmbbm.2013.08.022.
- [23] C. Giordano, S. Zappalà, S. Kleiven, Anisotropic finite element models for brain injury prediction: the sensitivity of axonal strain to white matter tract inter-subject variability, Biomech. Model. Mechanobiol. 16 (2017) 1269–1293, https://doi.org/ 10.1007/s10237-017-0887-5
- [24] W. Zhao, S. Ji, Cerebral vascular strains in dynamic head impact using an upgraded model with brain material property heterogeneity, J. Mech. Behav. Biomed. Mater. 126 (2022) 104967, https://doi.org/10.1016/j.jmbbm.2021.104967.
- [25] J.S. Giudice, A. Alshareef, T. Wu, A.K. Knutsen, L. V Hiscox, C.L. Johnson, M. B. Panzer, Calibration of a heterogeneous brain model using a subject-specific, Inverse Finite Element Approach 9 (2021) 1–17, https://doi.org/10.3389/fbios.2021.664268
- [26] W. Zhao, J.C. Ford, L.A. Flashman, T.W. McAllister, S. Ji, White matter injury susceptibility via fiber strain evaluation using whole-brain tractography, J. Neurotrauma 33 (2016) 1834–1847, https://doi.org/10.1089/neu.2015.4239.
- [27] Z. Zhou, X. Li, Y. Liu, M. Fahlstedt, M. Georgiadis, X. Zhan, S.J. Raymond, G. Grant, S. Kleiven, D. Camarillo, M. Zeineh, Toward a comprehensive delineation of white matter tract-related deformation, J. Neurotrauma 38 (2021) 3260–3278, https://doi.org/10.1089/neu.2021.0195.
- [28] H.T. Garimella, R.H. Kraft, Modeling the mechanics of axonal fiber tracts using the embedded finite element method, Int. j. Numer. Method. Biomed. Eng. 33 (2017) 26–35, https://doi.org/10.1002/cnm.2823.
- [29] W. Zhao, S. Ji, Incorporation of vasculature in a head injury model lowers local mechanical strains in dynamic impact, J. Biomech. 104 (2020) 109732.
- [30] H. Duckworth, A. Azor, N. Wischmann, K.A. Zimmerman, I. Tanini, D.J. Sharp, M. Ghajari, A finite element model of cerebral vascular injury for predicting microbleeds location, Front. Bioeng. Biotechnol. 10 (2022), https://doi.org/ 10.3389/fbioe.2022.860112.
- [31] X. Li, Subject-specific head model generation by mesh morphing: a personalization framework and its applications, Front. Bioeng. Biotechnol. 9 (2021), https://doi. org/10.3389/fbioe.2021.706566.
- [32] M. Ghajari, P.J. Hellyer, D.J. Sharp, Computational modelling of traumatic brain injury predicts the location of chronic traumatic encephalopathy pathology, Brain 140 (2017) 333–343, https://doi.org/10.1093/brain/aww317.
- [33] N. Atsumi, Y. Nakahira, E. Tanaka, M. Iwamoto, Human brain modeling with its anatomical structure and realistic material properties for brain injury prediction,

- Ann. Biomed. Eng. 46 (2018) 736–748, https://doi.org/10.1007/s10439-018-
- [34] Z. Zhou, X. Li, S. Kleiven, Biomechanics of periventricular injury, J. Neurotrauma (2019) 1–41. https://doi.org/10.1089/neu.2019.6634.
- [35] A. Alshareef, T. Wu, J.S. Giudice, M.B. Panzer, Toward subject-specific evaluation: methods of evaluating finite element brain models using experimental high-rate rotational brain motion, Biomech. Model. Mechanobiol. (2021) 1–17, https://doi. org/10.1007/s10237-021-01508-7.
- [36] N. Lin, S. Wu, S. Ji, A morphologically individualized deep learning brain injury model, J. Neurotrauma 40 (2023) 2233–2247, https://doi.org/10.1089/ neu.2022.0413.
- [37] X. Li, Z. Zhou, S. Kleiven, An anatomically accurate and personalizable head injury model: significance of brain and white matter tract morphological variability on strain, Biomech. Model. Mechanobiol. (2020) 1–29, https://doi.org/10.1101/ 2020.05.20.105635.
- [38] W. Zhao, S. Ji, Mesh convergence behavior and the effect of element integration of a human head injury model, Ann. Biomed. Eng. 47 (2019) 475–486, https://doi. org/10.1007/s10439-018-02159-z.
- [39] B. Rowson, S.M. Duma, A review of on-field investigations into the biomechanics of concussion in football and translation to head injury mitigation strategies, Ann. Biomed. Eng. (2020) 1–17, https://doi.org/10.1007/s10439-020-02684-w.
- [40] H. Ahmadzadeh, D.H. Smith, V.B. Shenoy, Viscoelasticity of tau proteins leads to strain rate-dependent breaking of microtubules during axonal stretch injury: predictions from a mathematical model, Biophys. J. 106 (2014) 1123–1133, https://doi.org/10.1016/j.bpj.2014.01.024.
- [41] H. Ahmadzadeh, D.H. Smith, V.B. Shenoy, Mechanical effects of dynamic binding between tau proteins on microtubules during axonal injury, Biophys. J. 109 (2015) 2328–2337, https://doi.org/10.1016/j.bpj.2015.09.010.
- [42] S.J. Peter, M.R.K. Mofrad, Computational modeling of axonal microtubule bundles under tension, Biophys. J. 102 (2012) 749–757, https://doi.org/10.1016/j. bpi.2011.11.4024.
- [43] J.P. Dollé, A. Jaye, S.A. Anderson, H. Ahmadzadeh, V.B. Shenoy, D.H. Smith, Newfound sex differences in axonal structure underlie differential outcomes from in vitro traumatic axonal injury, Exp. Neurol. 300 (2018) 121–134, https://doi. org/10.1016/j.expneurol.2017.11.001.
- [44] L.M. Wang, M.B. Goodman, E. Kuhl, Image-based axon model highlights heterogeneity in initiation of damage, Biophys. J. 122 (2023), https://doi.org/ 10.1016/j.bpj.2022.11.2946, 9–19. (Accessed 28 August 2023).
- [45] F. Zhu, D.L. Gatti, K.H. Yang, Nodal versus total axonal strain and the role of cholesterol in traumatic brain injury, J. Neurotrauma 33 (2016) 859–870, https://doi.org/10.1089/neu.2015.4007.
- [46] A. Montanino, S. Kleiven, Utilizing a structural mechanics approach to assess the primary effects of injury loads onto the axon and its components, Front. Neurol. 9 (2018) 643, https://doi.org/10.3389/fneur.2018.00643.
- [47] C. Zhang, S. Ji, Sex differences in axonal dynamic responses under realistic tension using finite element models, J. Neurotrauma 40 (2023) 2217–2232, https://doi. org/10.1089/NEU.2022.0512.
- [48] A. Montanino, X. Li, Z. Zhou, M. Zeineh, D.B. Camarillo, S. Kleiven, Subject-specific multiscale analysis of concussion: from macroscopic loads to molecular-level damage, Brain Multiphysics 2 (2021) 100027, https://doi.org/10.1016/j. hrain 2021 100027
- [49] M. Fahlstedt, F. Abayazid, M.B. Panzer, A. Trotta, W. Zhao, M. Ghajari, M. D. Gilchrist, S. Ji, S. Kleiven, X. Li, A.N. Annaidh, P. Halldin, Ranking and rating bicycle helmet safety performance in oblique impacts using eight different brain injury models, Ann. Biomed. Eng. 49 (2021) 1097–1109, https://doi.org/10.1007/pii/s1040-000-00708.prg
- [50] R. de Rooij, K.E. Miller, E. Kuhl, Modeling molecular mechanisms in the axon, Comput. Mech. 59 (2017) 523–537, https://doi.org/10.1007/s00466-016-1359-y.
- [51] S. Wu, W. Zhao, K. Ghazi, S. Ji, Convolutional neural network for efficient estimation of regional brain strains, Sci. Rep. 9 (2019) 17326, https://doi.org/ 10.1038/s41598-019-53551-1
- [52] K. Ghazi, S. Wu, W. Zhao, S. Ji, Instantaneous whole-brain strain estimation in dynamic head impact, J. Neurotrauma 38 (2021) 1023–1035, https://doi.org/ 10.1089/neu.2020.7281.
- [53] S. Wu, W. Zhao, S. Ji, Real-time dynamic simulation for highly accurate spatiotemporal brain deformation from impact, Comput. Methods Appl. Mech. Eng. 394 (2022) 114913, https://doi.org/10.1016/J.CMA.2022.114913.
- [54] X. Zhan, Y. Liu, S.J. Raymond, H.V. Alizadeh, A.G. Domel, O. Gevaert, M. M. Zeineh, G.A. Grant, D.B. Camarillo, Rapid estimation of entire brain strain using deep learning models, IEEE Trans. Biomed. Eng. 9294 (2021) 1–11, https://doi.org/10.1109/TBME.2021.3073380.
- [55] C. Deck, N. Bourdet, A. Trog, F. Meyer, V. Noblet, R. Willinger, Deep learning method to assess brain injury risk, Int. J. Crashworthiness (2022) 1–10, https://doi.org/10.1080/13588265.2022.2130600.
- [56] G.A. Truskey, The potential of deep learning to advance clinical applications of computational biomechanics, Bioengineering 10 (2023), https://doi.org/10.3390/ BIOENGINEERING10091066.
- [57] A. Ad, V. SS, C. P, C. T, E. AA, N. M, K. A, A Systematic Review on Machine Learning and Deep Learning Techniques in the Effective Diagnosis of Alzheimer's Disease, 2022, https://doi.org/10.21203/RS.3.RS-2028945/V1.
- [58] E. Courville, S.F. Kazim, J. Vellek, O. Tarawneh, J. Stack, K. Roster, J. Roy, M. Schmidt, C. Bowers, Machine learning algorithms for predicting outcomes of traumatic brain injury: a systematic review and meta-analysis, Surg. Neurol. Int. 14 (2023), https://doi.org/10.25259/SNI\_312\_2023.
- [59] A. Kaur, A.P.S. Chauhan, A.K. Aggarwal, Machine learning based comparative analysis of methods for enhancer prediction in genomic data, Int. Conf. Speech

- Technol. Human-Computer Dialogue (2019) 142–145, https://doi.org/10.1109/ICCT46177.2019.8969054.
- [60] R. Thukral, A.K. Aggarwal, A.S. Arora, T. Dora, S. Sancheti, Artificial intelligence-based prediction of oral mucositis in patients with head-and-neck cancer: a prospective observational study utilizing a thermographic approach, Cancer Res. Stat. Treat. 6 (2023) 181–190, https://doi.org/10.4103/CRST.CRST\_332\_22.
- [61] N. Lin, S. Wu, Z. Wu, S. Ji, Efficient generation of pretraining samples for developing a deep learning brain injury model via transfer learning, Ann. Biomed. Eng. (2023), https://doi.org/10.1007/S10439-023-03354-3 (in press).
- [62] S. Ji, W. Zhao, Displacement voxelization to resolve mesh-image mismatch: application in deriving dense white matter fiber strains, Comput. Methods Progr. Biomed. 213 (2022) 106528, https://doi.org/10.1016/j.cmpb.2021.106528.
- [63] S. Ji, W. Zhao, J.C. Ford, J.G. Beckwith, R.P. Bolander, R.M. Greenwald, L. A. Flashman, K.D. Paulsen, T.W. McAllister, Group-wise evaluation and comparison of white matter fiber strain and maximum principal strain in sports-related concussion, J. Neurotrauma 32 (2015) 441–454, https://doi.org/10.1089/peu.2013.3368
- [64] D. Sahoo, C. Deck, R. Willinger, Brain injury tolerance limit based on computation of axonal strain, Accid. Anal. Prev. 92 (2016) 53–70, https://doi.org/10.1016/j. aan 2016 03 013
- [65] A.K. Knutsen, A.D. Gomez, M. Gangolli, W.-T. Wang, D. Chan, Y.-C. Lu, E. Christoforou, J.L. Prince, P.V. Bayly, J.A. Butman, D.L. Pham, In vivo estimates of axonal stretch and 3D brain deformation during mild head impact, Brain Multiphysics (2020) 100015, https://doi.org/10.1016/j.brain.2020.100015.
- [66] L.F. Gabler, S.H. Huddleston, N.Z. Dau, D.J. Lessley, K.B. Arbogast, X. Thompson, J.E. Resch, J.R. Crandall, On-field performance of an instrumented mouthguard for detecting head impacts in American football, Ann. Biomed. Eng. 1–14 (2020), https://doi.org/10.1007/s10439-020-02654-2.
- [67] J. Tooby, D. Weaving, M. Al-Dawoud, G. Tierney, Quantification of head acceleration events in rugby league: an instrumented mouthguard and video analysis pilot study, Sensors 22 (2022) 584, https://doi.org/10.3390/S22020584.
- [68] E.M.P. Williams, F.J. Petrie, T.N. Pennington, D.R.L. Powell, H. Arora, K. A. Mackintosh, D.G. Greybe, Sex differences in neck strength and head impact kinematics in university rugby union players, Eur. J. Sport Sci. 22 (2022) 1649–1658, https://doi.org/10.1080/17461391.2021.1973573.
- [69] T.J. Fetchko, G.J. Hart, M.J. Aderman, J.D. Ross, S.R. Malvasi, M.H. Roach, K. L. Cameron, T.F. Rooks, Measurement of head kinematics using instrumented mouthguards during introductory boxing courses in U.S. Military academy cadets, Mil. Med. 188 (2023) 584–589, https://doi.org/10.1093/MILMED/USAD249.
- [70] E.E. Kieffer, M.T. Begonia, A.M. Tyson, S. Rowson, A two-phased approach to quantifying head impact sensor accuracy: in-laboratory and on-field assessments, Ann. Biomed. Eng. 48 (2020), https://doi.org/10.1007/s10439-020-02647-1.
- [71] B. Jones, J. Tooby, D. Weaving, K. Till, C. Owen, M. Begonia, K.A. Stokes, S. Rowson, G. Phillips, S. Hendricks, É.C. Falvey, M. Al-Dawoud, G. Tierney, Ready for impact? A validity and feasibility study of instrumented mouthguards (iMGs), Br. J. Sports Med. 56 (2022) 1171–1179, https://doi.org/10.1136/bjsports-2022-100722
- [72] S. Ji, S. Wu, W. Zhao, Dynamic characteristics of impact-induced brain strain in the corpus callosum, Brain Multiphysics 3 (2022) 100046, https://doi.org/10.1016/j. brain.2022.100046.
- [73] M. Cieslak, P.A. Cook, X. He, F.C. Yeh, T. Dhollander, A. Adebimpe, G.K. Aguirre, D.S. Bassett, R.F. Betzel, J. Bourque, L.M. Cabral, C. Davatzikos, J.A. Detre, E. Earl, M.A. Elliott, S. Fadnavis, D.A. Fair, W. Foran, P. Fotiadis, E. Garyfallidis, B. Giesbrecht, R.C. Gur, R.E. Gur, M.B. Kelz, A. Keshavan, B.S. Larsen, B. Luna, A. P. Mackey, M.P. Milham, D.J. Oathes, A. Perrone, A.R. Pines, D.R. Roalf, A. Richie-Halford, A. Rokem, V.J. Sydnor, T.M. Tapera, U.A. Tooley, J.M. Vettel, J. D. Yeatman, S.T. Grafton, T.D. Satterthwaite, QSIPrep: an integrative platform for preprocessing and reconstructing diffusion MRI data, Nat. Methods 187 (18) (2021) 775–778, https://doi.org/10.1038/s41592-021-01185-5.
- [74] N.J. Tustison, B.B. Avants, P.A. Cook, Y. Zheng, A. Egan, P.A. Yushkevich, J.C. Gee, N4ITK: improved N3 bias correction, IEEE Trans. Med. Imag. 29 (2010) 1310–1320, https://doi.org/10.1109/TMI.2010.2046908.
- [75] V. Fonov, A. Evans, R. McKinstry, C. Almli, D. Collins, Unbiased nonlinear average age-appropriate brain templates from birth to adulthood, Neuroimage 47 (2009) S102, https://doi.org/10.1016/s1053-8119(09)70884-5.
- [76] B.B. Avants, C.L. Epstein, M. Grossman, J.C. Gee, Symmetric diffeomorphic image registration with cross-correlation: evaluating automated labeling of elderly and neurodegenerative brain, Med. Image Anal. 12 (2008) 26–41, https://doi.org/ 10.1016/J.MEDIA.2007.06.004.
- [77] A.M. Dale, B. Fischl, M.I. Sereno, Cortical surface-based analysis. I. Segmentation and surface reconstruction, Neuroimage 9 (1999) 179–194, https://doi.org/ 10.1006/NIMG.1998.0395.
- [78] O. Esteban, C.J. Markiewicz, R.W. Blair, C.A. Moodie, A.I. Isik, A. Erramuzpe, J. D. Kent, M. Goncalves, E. DuPre, M. Snyder, H. Oya, S.S. Ghosh, J. Wright, J. Durnez, R.A. Poldrack, K.J. Gorgolewski, fMRIPrep: a robust preprocessing pipeline for functional MRI, Nat. Methods 161 (16) (2018) 111–116, https://doiorg/10.1038/s41592-018-0235-4.
- [79] J. Veraart, D.S. Novikov, D. Christiaens, B. Ades-aron, J. Sijbers, E. Fieremans, Denoising of diffusion MRI using random matrix theory, Neuroimage 142 (2016) 394–406, https://doi.org/10.1016/J.NEUROIMAGE.2016.08.016.
- [80] J.L.R. Andersson, S.N. Sotiropoulos, An integrated approach to correction for offresonance effects and subject movement in diffusion MR imaging, Neuroimage 125 (2016) 1063–1078, https://doi.org/10.1016/J.NEUROIMAGE.2015.10.019.
- 81] J.L.R. Andersson, S. Skare, J. Ashburner, How to correct susceptibility distortions in spin-echo echo-planar images: application to diffusion tensor imaging,

- Neuroimage 20 (2003) 870–888, https://doi.org/10.1016/S1053-8119(03)00336-7
- [82] J.D. Tournier, F. Calamante, D.G. Gadian, A. Connelly, Direct estimation of the fiber orientation density function from diffusion-weighted MRI data using spherical deconvolution, Neuroimage 23 (2004) 1176–1185, https://doi.org/10.1016/j. neuroimage.2004.07.037.
- [83] J.D. Tournier, C.H. Yeh, F. Calamante, K.H. Cho, A. Connelly, C.P. Lin, Resolving crossing fibres using constrained spherical deconvolution: validation using diffusion-weighted imaging phantom data, Neuroimage 42 (2008) 617–625, https://doi.org/10.1016/j.neuroimage.2008.05.002.
- [84] T. Dhollander, D. Raffelt, A. Connelly, Unsupervised 3-tissue response function estimation from single-shell or multi-shell diffusion mr data without a Coregistered T1 image, ISMRM Work. Break. Barriers Diffus. MRI (2016), 5:5.
- [85] T. Dhollander, R. Mito, D. Raffelt, A. Connelly, Improved white matter response function estimation for 3-tissue constrained spherical deconvolution, Intl. Soc. Mag. Reson. Med (2019) 555. https://archive.ismrm.org/2019/0555.html. (Accessed 25 November 2023).
- [86] D. Raffelt, T. Dhollander, J.-D. Tournier, R. Tabbara, R.E. Smith, E. Pierre, A. Connelly, Bias field correction and intensity normalisation for quantitative analysis of apparent fibre density, Proc. Intl. Soc. Mag. Reson. Med 25 (2017) 3541.
- [87] J.-D. Tournier, F. Calamante, A. Connelly, Improved probabilistic streamlines tractography by 2nd order integration over fibre orientation distributions, Proc. Int. Soc. Magn. Reson. Med. (2010) 1670. https://archive.ismrm.org/2010/1670. html. (Accessed 25 November 2023).
- [88] J.D. Tournier, R. Smith, D. Raffelt, R. Tabbara, T. Dhollander, M. Pietsch, D. Christiaens, B. Jeurissen, C.H. Yeh, A. Connelly, MRtrix3: a fast, flexible and open software framework for medical image processing and visualisation, Neuroimage 202 (2019), https://doi.org/10.1016/j.neuroimage.2019.116137.

- [89] W. Zhao, S. Ji, Displacement- and strain-based discrimination of head injury models across a wide range of blunt conditions, Ann. Biomed. Eng. 20 (2020) 1661–1677, https://doi.org/10.1007/s10439-020-02496-y.
- [90] W. Zhao, Z. Wu, S. Ji, Displacement error propagation from embedded markers to brain strain, J. Biomech. Eng. 143 (2021) 1–10, https://doi.org/10.1115/ 1.4051050
- [91] S. Rincon, R. Gupta, T. Ptak, Imaging of head trauma, Handb. Clin. Neurol. 135 (2016) 447–477, https://doi.org/10.1016/B978-0-444-53485-9.00022-2.
- [92] L. Henschel, S. Conjeti, S. Estrada, K. Diers, B. Fischl, M. Reuter, FastSurfer a fast and accurate deep learning based neuroimaging pipeline, Neuroimage 219 (2020), https://doi.org/10.1016/j.neuroimage.2020.117012.
- [93] L. Henschel, D. Kügler, M. Reuter, FastSurferVINN: building resolutionindependence into deep learning segmentation methods—a solution for HighRes brain MRI, Neuroimage 251 (2022), https://doi.org/10.1016/j. neuroimage.2022.118933.
- [94] G.Z. Voyiadjis, A. Samadi-Dooki, Hyperelastic modeling of the human brain tissue: effects of no-slip boundary condition and compressibility on the uniaxial deformation, J. Mech. Behav. Biomed. Mater. 83 (2018) 63–78, https://doi.org/ 10.1016/J.JMBBM.2018.04.011.
- [95] M. Hosseini-Farid, M. Ramzanpour, M. Ziejewski, G. Karami, A compressible hyper-viscoelastic material constitutive model for human brain tissue and the identification of its parameters, Int. J. Non Lin. Mech. 116 (2019) 147–154, https://doi.org/10.1016/J.IJNONLINMEC.2019.06.008.
- [96] S. Budday, G. Sommer, C. Birkl, C. Langkammer, J. Haybaeck, J. Kohnert, M. Bauer, F. Paulsen, P. Steinmann, E. Kuhl, G.A. Holzapfel, Mechanical characterization of human brain tissue, Acta Biomater. 48 (2017) 319–340, https://doi.org/10.1016/j.actbio.2016.10.036.
- [97] M. Soheilypour, M. Peyro, S.J. Peter, M.R.K. Mofrad, Buckling behavior of individual and bundled microtubules, Biophys. J. 108 (2015) 1718–1726, https://doi.org/10.1016/j.bpj.2015.01.030.